Chemical Physics 535 (2020) 110794

Contents lists available at ScienceDirect

Chemical Physics

journal homepage: www.elsevier.com/locate/chemphys

Vibrational and distorted-wave effects on the highest occupied molecular orbital electronics structure of tetrachloromethane

Li Ding[a], Enliang Wang[b,*], Zhongfeng Xu[a], Yufan Wu[a], Jingkang Deng[c], Chuangang Ning[c], Xueguang Ren[a,b,*]

[a] School of Science, Xi'an Jiaotong University, Xi'an 710049, China
[b] Max Planck Institut für Kernphysik, Saupfercheckweg 1, 69117 Heidelberg, Germany
[c] Department of Physics, State Key Laboratory of Low-Dimensional Quantum Physics, Tsinghua University, Beijing 100084, China

ARTICLE INFO

Keywords:
Electronic structure
CCl_4
HOMO
Distorted-wave
Vibrational effect

ABSTRACT

In this work, we study the valence orbital momentum profiles of tetrachloromethane (CCl_4) performed with binary (e, 2e) measurements at the impact energies of about 600 and 1200 eV with higher energy-resolution of $\Delta\varepsilon\sim0.7$ eV. The experimental momentum profiles for the molecular orbitals , and $6a_1$ are obtained and compared with calculations under the plane-wave impulse approximation. The calculations at the equilibrium geometry of CCl_4 show generally good agreement with the experimental momentum profiles except for the low momentum range of $2t_1$ and $2e$ which is considerable lower than the experiment. The experimental momentum profile shows dynamic dependencies on the impact energies which is ascribed to the distorted-wave effects. Further calculation considering molecular vibrations for the $2t_1$ highest occupied molecular orbital (HOMO) shows a better agreement with experiment than the equilibrium calculation, indicating the important role of nuclear motions on the HOMO electronic structure of CCl_4.

1. Introduction

Electron momentum spectroscopy (EMS), based on the binary (e, 2e) ionization reaction near the Bethe ridge, is now a well-established technique for the investigation of the valence electronic structure of atoms, molecules, and condensed matter [1–5]. The basic information obtained from EMS are the binding energy spectra (BES) over a wide energy range usually covering the complete valence shell, and angular distributions of (e, 2e) cross section for individual transitions giving rise to the peaks in BES. Within the plane wave impulse approximation (PWIA) and the target Hartree-Fock or target Kohn-Sham approximation, the measured (e, 2e) cross section is proportional to the spherically averaged momentum profile of a specific molecular orbital [1]. Furthermore, since electron momentum profile is sensitive to diffuse parts of the position wave function, EMS can provide information relevant to issues of chemical reaction and molecular recognition, and the momentum space electron density may be a criterion for molecular similarity and dissimilarity [6].

Tetrachloromethane or CCl_4 is an organo-chlorinated compound. It has a role as a refrigerant and a hepatotoxic agent and remains important intermediates and products of the chemical process industries. It is also a weak greenhouse gas, contributing to global warming [7]. In chemistry, the highest occupied molecular orbital (HOMO) plays a determining role in directing chemical reactivity of molecules like CCl_4 [8]. Therefore the studies of binding energy and orbital electron density distribution of CCl_4 by EMS experiments and related theoretical calculations are of great relevance for our understanding of the electronic and molecular structure of the reactant molecules [9].

Previous experiments of CCl_4 have been carried out using EMS by Watanabe et al. [10] and Grisogono et al. [7] in which the valence orbital momentum profiles and bond oscillation effects have been reported. In these studies, however, the three outermost orbitals (i.e. $2t_1$, $7t_2$ and $2e$) were not resolved in BES due to the limited energy-resolutions. Since the outermost orbitals, also known as frontier orbitals, are very important for many chemical and physical properties concerning particularly the chemical reactions [8]. It would be interesting and potentially fruitful if the outermost orbitals can be individually studied by high-resolution EMS experiment in order to obtain the detailed electronic structure information for each orbital. Furthermore, recent EMS studies have shown that the electron momentum profiles of molecules can be influenced by distorted-wave effect [11–17] and molecular vibration [18–21]. It is also important to analyze these effects for better understanding of the measured momentum profiles.

In the present work, we report the valence orbital momentum

* Corresponding authors at: School of Science, Xi'an Jiaotong University, Xi'an 710049, China (X. Ren).
E-mail addresses: enliang.wang@mpi-hd.mpg.de (E. Wang), renxueguang@xjtu.edu.cn (X. Ren).

https://doi.org/10.1016/j.chemphys.2020.110794
Received 28 November 2019; Received in revised form 21 March 2020; Accepted 5 April 2020
Available online 07 April 2020

profiles of CCl_4 measured at the impact energies of about 600 and 1200 eV using a symmetric noncoplanar binary (e, 2e) spectrometer. The binding energy spectra were measured with higher energy-resolution of $\Delta\varepsilon\sim$ 0.7 eV (full width at half maximum, FWHM) for energy range from 8 to 43 eV. The experimental momentum profiles for the individual $2t_1$, $7t_2$, $2e$, $6t_2$, and $6a_1$ orbitals are obtained and compared with theoretical momentum profiles. They are calculated at the equilibrium geometry of CCl_4 as well as using the thermal sampling molecular dynamics method to consider molecule vibrational effect [21]. For $2t_1$ HOMO, the calculation considering molecular vibrations are in better agreement with experiment than the equilibrium geometry calculations. The distortion wave effects are observed in the experimental momentum profiles of $2t_1$ and $2e$ which display dynamic dependencies on the impact energies. A multi-center interference or bond oscillation effect has been observed from the momentum profile ratios of $2t_1$ to $7t_2$ and $2e$ to $7t_2$.

2. Experimental setup

EMS is based on the high-energy electron impact ionization process. An incident electron with energy E_0 causes the target molecule to be ionized. By detecting the two outgoing (scattered and ejected) electrons in coincidence, the kinematics of the reaction can be completely determined. The experiment was performed using a high-resolution and high-sensitivity electron momentum spectrometer. The details of this apparatus have been reported in previous works [22–24], so only a brief description will be given here. The experiment utilizes a non-coplanar symmetric geometry[22], i.e., the two outgoing electrons have almost equal energies and equal polar angles($\theta_a \approx \theta_b = 45°$) with respect to the direction of the incident electron beam. The electron beam is generated by an electron gun equipped with an oxide cathode (0.3 eV energy spread) and was ejected into the reaction zone to collide with the diffuse CCl_4 gas target. A double toroidal energy analyzer is equipped with two position- and time-sensitive detectors to detect the two outgoing electrons in coincidence. A wide range of electron energies and out-of-plane azimuthal angles were measured in the experiment. Therefore, the data acquisition efficiency is greatly increased with respect to conventional single energy and angle detection techniques. The binding energy resolution in the present work is about 0.7 eV (FWHM), and angular resolutions are $\Delta\theta = \pm 0.6°$, $\Delta\phi = \pm 0.85°$ respectively, which were obtained with a calibration measurement on argon.

In experiment, the binding energy ε and recoil ion momentum $\vec{q}$ can be determined by means of the energy and momentum conservation laws:

$$\varepsilon = E_0 - E_a - E_b, \tag{1}$$

$$\vec{q} = \vec{p_0} - \vec{p_a} - \vec{p_b}. \tag{2}$$

Here E_i and $\vec{p_i}$ (i = 0, a, b) are the energies and momenta of the incident, scattered, and ejected electrons, respectively. Under the conditions of high-energy and high momentum-transfer, and the approximation of binary encounter, the recoil-ion momentum $\vec{q}$ can be equal in magnitude but opposite in sign to the target bound electron momentum $\vec{p}$ [1]. The magnitude of the electron momentum $\vec{p}$ is related to the out-of-plane azimuthal angle ϕ between the two outgoing electrons:

$$p = \left\{(p_0 - \sqrt{2}p_a)^2 + 2p_a^2 \sin(\frac{\phi}{2})^2\right\}^{1/2}. \tag{3}$$

3. Theoretical background

The EMS reaction theory is based on several approximations through which the (e, 2e) cross-section is related to the electron momentum profile [1–5]. Of these the most important are the binary encounter approximation and the plane-wave impulse approximation. In order to ensure the validity of these approximations the experiment has to be conducted under what are known as EMS conditions, which are sufficiently high electron impact energy and, optimally, the use of the symmetric non-coplanar kinematics. Under these conditions the kinematics factors are effectively constant, the EMS cross-section for randomly oriented molecules can be given by:

$$\sigma_{EMS} \propto \int d\Omega |\langle p\Psi_f^{N-1}|\Psi_i^N\rangle|^2 \tag{4}$$

where p is the momentum of the target electron prior to be ejected. Ψ_f^{N-1} and Ψ_i^N are the total electronic wave functions for the final ion state and the target molecule ground (initial) state, respectively. The overlap of the ion and neutral wave functions in Eq. (4) is known as the Dyson orbital while the square of this quantity is referred to as an ion-neutral overlap distribution. Under the target Hartree-Fock approximation (THFA) or the target Kohn-Sham approximation (TKSA), the EMS cross section can be simplified [1] by:

$$\sigma_{EMS} \propto S_i^f \int d\Omega |\psi_i(p)|^2 \tag{5}$$

where $\psi_i(p)$ is the momentum space representation of a canonical Hartree-Fock or Kohn-Sham orbital wavefunction, and S_i^f denotes the associated spectroscopic factor or pole strength, which accounts for the shake-up processes due to configuration interactions in the final state. The integrals in Eqs. (4) and (5) are known as the spherically averaged one-electron momentum profile. Therefore, EMS has the ability to image the electron density distribution in individual orbital selected according to their binding energies.

Usually, the electron momentum profile is obtained at the equilibrium geometry of the molecule. With the help of modern high performance computer, the influence of molecular vibration on electronic structure can be analyzed which is based on the vertical ionization at fixed molecular geometry, however, it is distorted by the thermal energy. The vibrational effect can be accounted for by using the analytical method like the so-called Harmonic Analytical Quantum Mechanical (HAQM) [18]. Here, a thermal sampling molecular dynamics (TSMD) method is used to consider the vibrational effects in EMS [21]. In brief, considering the molecular vibrational effect, the electron momentum profile at fixed molecular geometry can be expressed as,

$$\sigma_{EMS} \propto \frac{1}{N}\sum_j^N \sum_v P_v(T)|\chi_{iv}(Q_j)|^2 S_i^f \int d\Omega |\psi_i(p, Q_j)|^2 \Delta Q_j, \tag{6}$$

where $P_v(T)$ is population of initial vibrational state, v, at temperature T which can be determined by the Boltzmann distribution. $\chi_{iv}(Q)$ is the vibrational wavefunctions of the initial state Q_j being the sampled molecular geometry. j means the number of the sampled molecular geometry. The populations of the vibrational states are sampled using Boltzmann distribution. Such a procedure is usually referred to as a thermal sampling process, which simulates the molecular rotation-vibration under certain temperatures T. In this work, the influence of thermal energy to molecular geometry is analyzed and sampled using quasiclassical fixed normal-mode sampling method [25]. The temperature of diffusive gas target is assumed to be about 300 K (room temperature) which is adopted in the calculation.

4. Results and discussion

The CCl_4 molecule is tetrahedral structure and the point group symmetry is T_d. Its ground state electronic configuration at B3LYP/aug-cc-pVTZ level can be written as,

$$(core)^{42}(5a_1)^2(5t_2)^6(6a_1)^2(6t_2)^6(2e)^4(7t_2)^6(2t_1)^6.$$

The position space molecular orbital diagram of CCl_4 valence orbitals are presented in Fig. 1. The three outermost orbitals of CCl_4 consist mainly of the 3p lone-pair orbitals of Cl atoms. For these three MOs, the

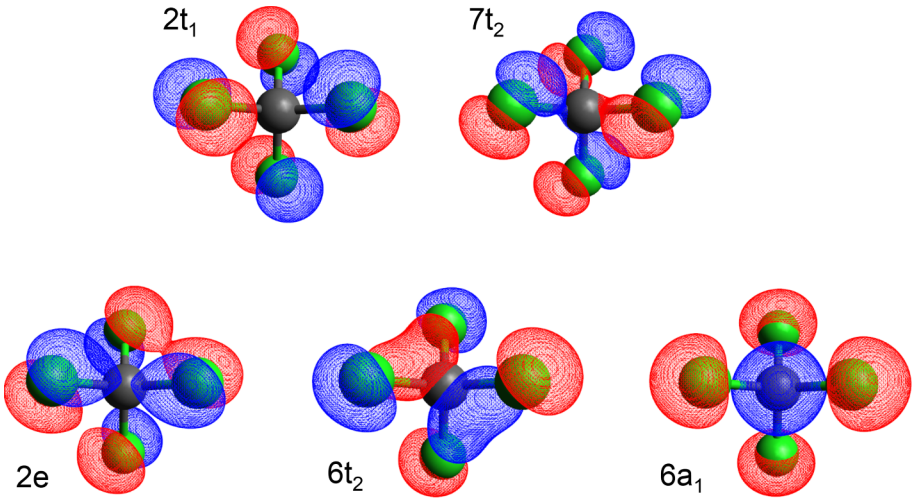

Fig. 1. Maps of the outer-valence molecular orbitals of CCl_4.

multi-center interference effect [10,26,27], i.e. the bond oscillatory, is expected to be observed. Here, except for the $6a_1$ orbital, the electron density is mainly distributed among the four Cl atoms.

4.1. Binding-energy spectra

Fig. 2 presents the experimental angle-resolved binding-energy spectra (BES) of CCl_4 measured at an impact energy of about 1200 eV. In the experiment, the BES of different ϕ angles can be obtained simultaneously. From the angle-energy density map shown in Fig. 2(a), the basic features of EMS for each outer valence orbital can be seen clearly. It is shown that, except for the $6a_1$ orbital, the minimum density of each orbit is observed at the azimuth angle $\phi = 0°$, i.e. the momentum origin ($p\sim 0$ a.u.). The main reason is that the C 2s state contributes to the $6a_1$ orbital, while the other states mainly contain the Cl 3p state. The BES obtained by summing all the energy spectra of different ϕ angles was shown in Fig. 2(b). The outer valence orbital ionization contributes to the peaks at binding energy range of 10–22.5 eV in which the electron correlation induced shake-up process can be ignored. For the peaks above 25 eV, the contribution from inner valence ionization and the shake-up processes are comparable. The theoretical bind energy spectrum is calculated using the symmetry-adapted-cluster configuration-interaction (SAC-CI) general-R [28–30] method with cc-pVDZ basis set as shown in Fig. 2(c). The positions and heights of the blue vertical bars correspond to the ionization potential and pole strength of the corresponding Dyson orbitals. For the sake of comparison, the experimental energy resolution (0.7 eV) is convoluted. The simulated spectrum can well reproduce the feature of the measured one.

The experimental momentum profile of each orbital was obtained by fitting the combined energy spectrum at different ϕ angles with multiple Gaussian functions. The peak centers were determined through high-resolution photoelectron spectroscopy (PES) [31], and the widths were determined by combining the experimental energy resolution and the vibrational broadening on PES. The experimental momentum profiles were obtained by fitting the intensity for each state plotted as a function of the momentum p. In this work, the experimental error bars of electron momentum profiles include both of the statistical, and deconvolution uncertainties.

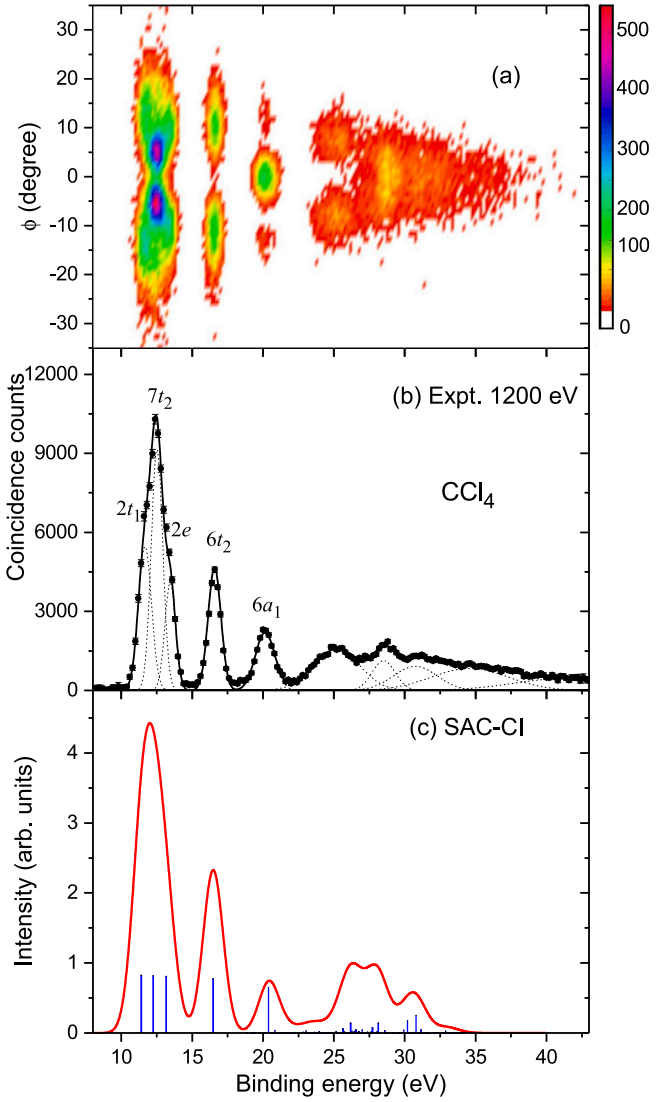

Fig. 2. (a) Experimental momentum-energy density map of CCl_4 and (b) binding-energy spectrum summed over all azimuthal angles ϕ obtained at the impact energy of 1200 eV plus binding energies. The dashed lines represent Gaussian fits to the individual peaks and the solid curve is the summed fit. The labels are the outer-valence orbital assignments. (c) Simulated binding energy spectrum by SAC-CI general-R method.

4.2. Electron momentum profiles

The electron momentum profiles for the individual valence orbitals of CCl_4 are shown in Fig. 3. The $2t_1$, $7t_2$, and $2e$ orbitals are mainly constructed from the Cl 3p lone-pair atomic orbitals. These orbitals

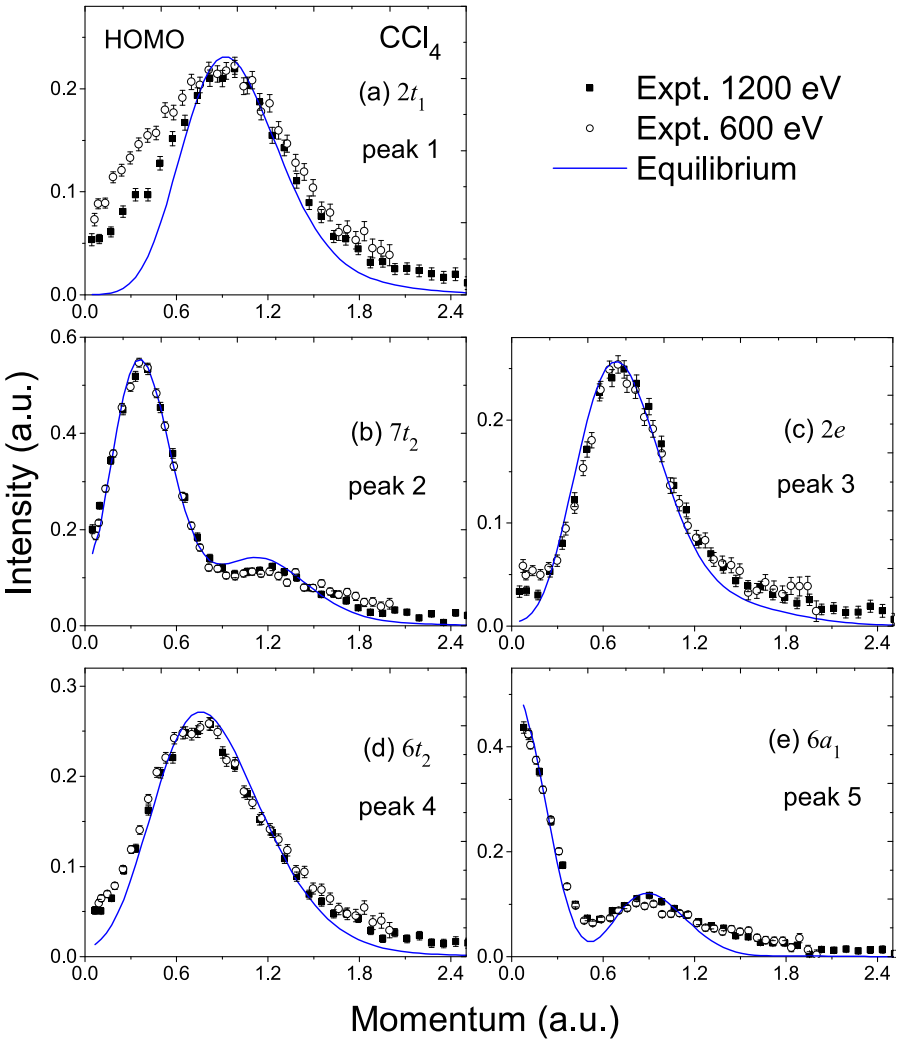

Fig. 3. Measured electron momentum profiles for the outer valence orbitals of CCl_4 at the impact energies of 600 and 1200 eV in comparison with the calculated ones. The solid curves are calculations at the equilibrium geometry of CCl_4.

show a *p*-type feature on the momentum profiles. The $7t_2$ orbital shows a double *p*-type feature with two maximum at $p \sim 0.4$ and 1.2 a.u. For $2t_1$ and $2e$, they show *p*-type feature, and the peak values are at about 1.0 and 0.7 a.u., respectively. The differences between these three orbitals originate from the different orientations of the 3p lone-pair of Cl. As shown in Fig. 1, two antiparallel 3p lone-pairs contribute to the orbital of $2t_1$ from the left-lower and right-upper sides two Cl. The orbital of $2e$ is also contributed from left-upper and right-lower sides of Cl. For these two orbitals, there is only a small phase shift in their momentum distribution. However, for the $7t_2$ orbital, four almost parallel lone-pairs of Cl contribute to this orbital, which is expected to show an antiphase feature relative to $2t_1$ and $2e$'s momentum distribution. The $6t_2$ and $6a_1$ orbitals are contributed by covalent bonds between C and Cl atoms. The $6t_2$ orbital show a *p*-type momentum profile with a maximum value of 0.7 a.u. While the $6a_1$ orbital exhibit *sp*-type feature with two maximum values located at the origin of momentum ($p \sim 0$ a.u.) and $p \sim 0.8$ a.u., respectively.

The experimental momentum profiles of the $2t_1$, $7t_2$, $2e$, $6t_2$, and $6a_1$ orbitals are shown in Fig. 3(a)–(e), respectively, and compared with the theoretical calculations at the equilibrium geometry. The experimental data are generally well described by the calculated momentum profiles at the equilibrium geometry especially for $7t_2$, $6t_2$ and $6a_1$ orbitals. The results for $6t_2$ and $6a_1$ orbitals are also consistent with the previous EMS study of CCl_4 [10]. For $2t_1$ and $2e$ orbitals, however, the experimental data at low momenta show higher intensity than the theoretical momentum profiles. This is the so-called turn-up effect and can be qualitatively assigned to the distortion effect of incident and outgoing electron waves in the target and ion potential since the observed turn-up effects show dynamic dependencies on the impact energies [11–17]. The observed discrepancy between experiment and theory become smaller at 1200 eV impact energy. At present, appropriate theoretical calculations using distorted wave in molecules are still very challenging at high energy due to the multi-center nature [11].

4.3. Vibrational effect

For the small *p* region, recent studies have shown that molecular vibration may considerably affect momentum profiles [18–21]. Here, the vibration is related to the influence of nuclear motion on the geometry of molecular structure, and thus the electron density of the individual orbitals, which can be analyzed by molecular dynamical simulation. We thus performed an additional calculation for the $2t_1$ HOMO, which takes vibrational effects into account using a TSMD method. The vibrational calculation of the $2t_1$ HOMO momentum profile is presented in Fig. 4 which shows better agreement with the experimental data at low momenta than the equilibrium geometry result. This indicates that the nuclear motion can influence the HOMO electronic structure of CCl_4 molecule.

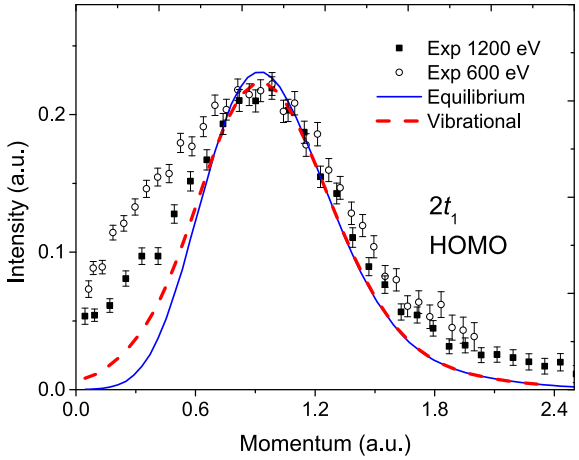

Fig. 4. Calculated momentum profile for $2t_1$ HOMO using a TSMD method to consider the molecule vibrational effect (thick dashed curve). The experimental data at the impact energies of 600 and 1200 eV and calculation at the equilibrium geometry (thin solid curve) are also included for comparisons.

It can be seen from the comparison between experiment and theory that molecular vibration is responsible at roughly ~30% for the observed turn-up effect of the $2t_1$ orbital momentum profiles. In comparison with the previous work of Xu et al. [21] where the molecular vibration affects all of the outer-valence orbits of CBr_4, especially, the vibrational effect can almost completely explain the turn-up effect for $13t_2$, $12t_2$, and $9a_1$ orbitals of CBr_4, the present work shows that such effect only affects the HOMO of CCl_4. For the other orbitals of CCl_4, the molecular vibration effect can be ignored. Usually, replacing one halogen element by another in the same molecule type is expected to produce a same momentum profile due to that CBr_4 and CCl_4 have almost the same outer-valence electronic structure. This work shows that different halogen elements may induce different vibrational and distorted-wave effect. The distorted-wave effect in CCl_4 is stronger than that in CBr_4. This may due to that the Br has many more electrons than Cl which leads to a better shielding effect on the nucleus potential.

The even higher impact energy experiment and high energy distorted-wave calculation are required. The remaining discrepancy between vibrational calculation and 1200 eV experimental data may be eliminated if both molecular vibration and distorted-wave effects can be considered in theory [32,33] or the distortion wave effect can be further removed by increasing the impact energy to higher than 4000 eV in experiment [34].

4.4. Bond oscillation effect

The molecular orbital in momentum space can be described as a linear combination of atomic orbitals, the information about the equilibrium nuclear position $\boldsymbol{R}_j$ is presented in the phase factors of $\exp(i\boldsymbol{p}\cdot\boldsymbol{R}_j)$. As a result the momentum profile reveals an oscillation behavior, which is referred to as multi-center interference or bond oscillation effect [10,26,27]. For CCl_4 molecule, the $2t_1$, $7t_2$ and $2e$ orbitals are mainly composed of 3p lone pair orbitals of Cl, and it is expected that they will involve the bond oscillation effect. At present, we study the bond oscillation effects by plotting the ratio of two orbitals with antiphase feature in the momentum distributions, namely $2t_1/7t_2$ and $2e/7t_2$. This provides an alternative method of extracting a multi-center interference pattern in which the oscillation structures can be amplified [27].

The antiphase features of $2t_1/7t_2$ and $2e/7t_2$ are clearly visible on the logarithmic scale momentum profiles as shown in Fig. 5(a). The experimental ratios at the impact energies of 1200 eV are presented in Fig. 5(b) and (c) for $2t_1/7t_2$ and $2e/7t_2$, respectively. Equilibrium geometry calculations are also included in the figures. The momentum

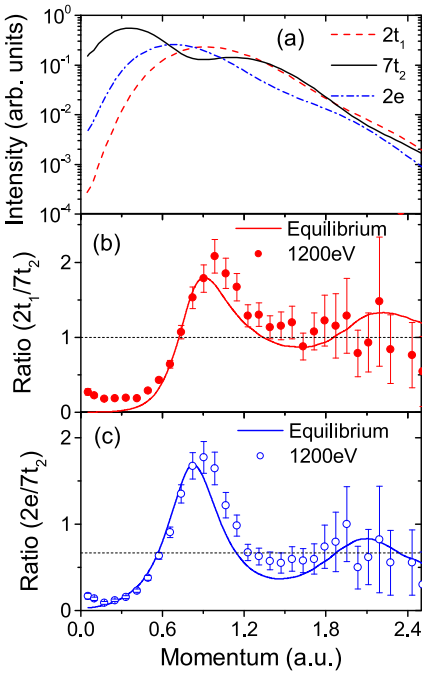

Fig. 5. The momentum profiles for $2t_1$, $7t_2$ and $2e$ orbitals in logarithmic scale (a), and the momentum profile ratios for $2t_1/7t_2$ (b) and $2e/7t_2$ (c).

profile ratios show a significant oscillations near a constant value, which is a clear evidence of multi-center interference effect. The constant ratios are determined by the number of electrons occupied in each molecular orbital, that is 1 for $2t_1/7t_2$ and 2/3 for $2e/7t_2$. The experimental ratios are in good agreement with theoretical calculations both in magnitudes and peak positions.

The momentum profile ratio is very sensitive to the interatomic distance [27]. In order to determine the exact value of the bond length from the experimental data, theoretical momentum profile ratios are calculated at different interatomic distances R and a least-square fitting method is performed. The function of the least-square fitting is defined as,

$$\chi^2(R,\alpha) = \frac{1}{N}\sum_i^N [\alpha\rho_{\text{the}}(R,p_i) - \rho_{\text{exp}}(p_i)]^2 \tag{7}$$

where ρ_{the} and ρ_{exp} are the theoretical and experimental momentum profile ratios. R is the interatomic distance and α is the scaling factor of the theoretical momentum profile ratio. The χ^2 distribution is shown in Fig. 6 where the two ratios, i.e. $2t_1/7t_2$ and $2e/7t_2$ are averaged. The minimum point is found at $(R\text{-}R_{eq})/R_{eq} = -1.5\%$. Finally, the bond length of CCl_4 is determined, $R_{C-Cl} = 1.76 \pm 0.14$ Å.

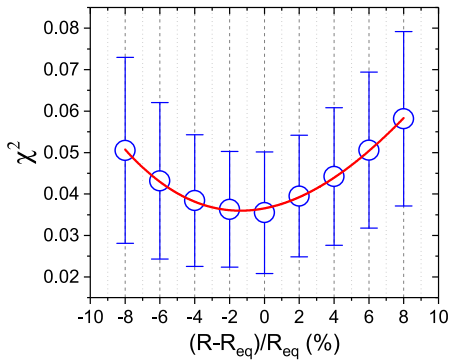

Fig. 6. Te χ^2 value distribution as a function of interatomic distances.

5. Conclusion

We have reported a combined experimental and theoretical study of the valence electronic structure of tetrachloromethane (CCl_4) by electron momentum spectroscopy (EMS). The binding-energy spectrum (BES) for the energy range from 8 to 43 eV were measured with higher energy-resolution of $\Delta\varepsilon \sim 0.7$ eV, and thus, the three outermost $2t_1$, $7t_2$, $2e$ orbitals are resolved in BES. The momentum profiles of valence orbitals were measured with a high-sensitivity binary (e, 2e) spectrometer at impact energies of about 600 and 1200 eV.

The experimental momentum profiles of individual $2t_1$, $7t_2$, $2e$, $6t_2$, and $6a_1$ orbitals are compared with the theoretical profiles calculated at the equilibrium geometry of CCl_4 which show rather good agreement with the experimental data. At low momenta (p 0.7 a.u.), however, there is an unexpected higher intensity in comparison with the equilibrium calculations for $2t_1$ and $2e$ orbitals. The observed discrepancies at low momenta can be partially explained by the distorted-wave effect since the size of the effect decreases with the increasing of the impact-energy. Moreover, we performed an additional calculation for the $2t_1$ highest occupied molecular orbital (HOMO), which consider the molecule vibrational effect using the thermal sampling molecular dynamics (TSMD) method (1000 thermal sampling geometries). The vibrational calculation shows better agreement with the experimental momentum profiles than the equilibrium calculation. This indicates the important role of nuclear motion on the HOMO electronic structure of CCl_4.

It is also to be noted that the present calculations are far from satisfactory for reproducing the higher intensity observed at low momenta of $2t_1$ HOMO orbital. More sophisticated models considering distorted-wave approximation for all the incoming and outgoing electrons [32,33,35–37] are expected to fully describe the experimental (e, 2e) momentum profiles of CCl_4 molecule. Finally, we study the bond oscillation effect in the lone-pair orbitals of $2t_1$, $7t_2$ and $2e$ using the electron momentum profiles ratios for $2t_1$ to $7t_2$ and $2e$ to $7t_2$. The experimental ratios are in good agreement with the theoretical calculation, and the oscillatory structure is clearly revealed for the outermost orbitals.

Declaration of Competing Interest

The authors declare that they have no known competing financial interests or personal relationships that could have appeared to influence the work reported in this paper.

CRediT authorship contribution statement

Li Ding: Data curation, Investigation, Writing - original draft. **Enliang Wang:** Supervision, Writing - review & editing. **Zhongfeng Xu:** Data curation, Investigation. **Yufan Wu:** Data curation, Investigation. **Jingkang Deng:** Data curation, Investigation. **Chuangang Ning:** Data curation, Investigation. **Xueguang Ren:** Supervision, Writing - review & editing.

Acknowledgment

This work was supported by the National Natural Science Foundation of China under Grant Nos. 11774281 and 11875219. E.W. acknowledges a fellowship from the Alexander von Humboldt Foundation.

References

[1] I.E. McCarthy, E. Weigold, Electron momentum spectroscopy of atoms and molecules, Rep. Prog. Phys. 54 (6) (1991) 789 URL http://stacks.iop.org/0034-4885/54/i=6/a=001.
[2] C.E. Brion, Looking at orbitals in the laboratory: the experimental investigation of molecular wavefunctions and binding energies by electron momentum spectroscopy, Int. J. Quantum Chem. 29 (5) (1986) 1397–1428, https://doi.org/10.1002/qua.560290534.
[3] M.A. Coplan, J.H. Moore, J.P. Doering, (e, 2e) spectroscopy, Rev. Mod. Phys. 66 (1994) 985–1014, https://doi.org/10.1103/RevModPhys.66.985.
[4] M. Vos, I.E. McCarthy, Observing electron motion in solids, Rev. Mod. Phys. 67 (1995) 713–723, https://doi.org/10.1103/RevModPhys.67.713.
[5] M. Takahashi, Looking at molecular orbitals in three-dimensional form: From dream to reality, Bull. Chem. Soc. Jpn. 82 (7) (2009) 751–777, https://doi.org/10.1246/bcsj.82.751.
[6] D.L. Cooper, N.L. Allan, Molecular dissimilarity: a momentum-space criterion, J. Am. Chem. Soc. 114 (12) (1992) 4773–4776, https://doi.org/10.1021/ja00038a048.
[7] A. Grisogono, R. Pascual, W. von Niessen, E. Weigold, The polychloromethanes – an experimental and theoretical investigation of their valence electronic structure, Chem. Phys. 135 (3) (1989) 317–346, https://doi.org/10.1016/0301-0104(89)80110-7 URL: http://www.sciencedirect.com/science/article/pii/0301010489801107.
[8] K. Fukui, The role of frontier orbitals in chemical reactions (nobel lecture), Angewandte Chemie International Edition in English 21 (11) (1982) 801–809, https://doi.org/10.1002/anie.198208013 URL: https://onlinelibrary.wiley.com/doi/abs/10.1002/anie.198208013.
[9] C. Brion, G. Cooper, Y. Zheng, I. Litvinyuk, I. McCarthy, Imaging of orbital electron densities by electron momentum spectroscopy a chemical interpretation of the binary (e,2e) reaction, Chem. Phys. 270 (1) (2001) 13–30, https://doi.org/10.1016/S0301-0104(01)00385-8 URL: http://www.sciencedirect.com/science/article/pii/S0301010401003858.
[10] N. Watanabe, K. Katafuchi, M. Yamazaki, M. Takahashi, Interference effects on (e, 2e) electron momentum profiles: acomparative study for ccl4 and cf4*, Eur. Phys. J. D 70 (12) (2016) 268, https://doi.org/10.1140/epjd/e2016-70516-7.
[11] X. Wang, S. Xu, C. Ning, O. Al-Hagan, P. Hu, Y. Zhao, Z. Xu, J. Deng, E. Wang, X. Ren, A. Dorn, D. Madison, Dynamic effects in electron momentum spectroscopy of sulfur hexafluoride, Phys. Rev. A 97 (2018) 062704, https://doi.org/10.1103/PhysRevA.97.062704.
[12] C.E. Brion, Y. Zheng, J. Rolke, J.J. Neville, I.E. McCarthy, J. Wang, Distorted-wave effects at low momentum in binary (e, 2e) cross sections for d-orbital ionization, J. Phys. B: Atomic Mol. Opt. Phys. 31 (5) (1998) L223 URL http://stacks.iop.org/0953-4075/31/i=5/a=003.
[13] X.G. Ren, C.G. Ning, J.K. Deng, S.F. Zhang, G.L. Su, F. Huang, G.Q. Li, Direct observation of distorted wave effects in ethylene using the (e, 2e) reaction, Phys. Rev. Lett. 94 (2005) 163201, https://doi.org/10.1103/PhysRevLett.94.163201.
[14] M. Zhao, X. Shan, S. Niu, X. Chen, Relativistic and distorted wave effects on xe 4d electron momentum distributions, Chin. Phys. B 26 (9) (2017) 093103 URL http://stacks.iop.org/1674-1056/26/i=9/a=093103.
[15] X.G. Ren, C.G. Ning, J.K. Deng, G.L. Su, S.F. Zhang, Y.R. Huang, (e, $2e$) study on distorted-wave and relativistic effects in the inner-shell ionization processes of xenon $4d_{5/2}$ and $4d_{3/2}$, Phys. Rev. A 73 (2006) 042714, https://doi.org/10.1103/PhysRevA.73.042714.
[16] S. Xu, C. Ma, E. Wang, P. Hu, X. Wang, Y. Zhao, Z. Xu, J. Deng, C. Ning, A. Dorn, X. Ren, Observation of strong relativistic and distorted-wave effects in (e,2e)) electron-momentum spectroscopy of mercury, Phys. Rev. A 99 (2019) 022705, https://doi.org/10.1103/PhysRevA.99.022705.
[17] X. Ren, C. Ning, J. Deng, S. Zhang, G. Su, F. Huang, G. Li, Sensitive observations of orbital electron density image by electron momentum spectroscopy with different impact energies, Chem. Phys. Lett. 404 (4) (2005) 279–283, https://doi.org/10.1016/j.cplett.2005.01.100 URL: http://www.sciencedirect.com/science/article/pii/S0009261405001454.
[18] N. Watanabe, M. Yamazaki, M. Takahashi, Vibrational effects on valence electron momentum distributions of ethylene, J. Chem. Phys. 137 (11) (2012) 114301, https://doi.org/10.1063/1.4752653.
[19] Y. Tang, X. Shan, J. Yang, S. Niu, Z. Zhang, N. Watanabe, M. Yamazaki, M. Takahashi, X. Chen, Vibrational effects on electron momentum distributions of outer-valence orbitals of oxetane, J. Phys. Chem. A 120 (34) (2016) 6855–6863, https://doi.org/10.1021/acs.jpca.6b06706.
[20] Z. Li, Y. Tang, Z. Liu, S. Niu, X. Shan, X. Chen, Electron momentum spectroscopy study of outer valence electronic structure of pyrrole, Chem. Phys. 517 (2019) 54–59, https://doi.org/10.1016/j.chemphys.2018.09.041 URL: http://www.sciencedirect.com/science/article/pii/S0301010418309054.
[21] Z. Xu, P. Hu, E. Wang, S. Xu, X. Wang, Y. Zhao, J. Deng, C. Ning, X. Ren, Experimental and theoretical study of valence electronic structure of tetrabromomethane by (e,2e) electron momentum spectroscopy, Phys. Rev. A 99 (2019) 062705, https://doi.org/10.1103/PhysRevA.99.062705.
[22] X.G. Ren, C.G. Ning, J.K. Deng, S.F. Zhang, G.L. Su, F. Huang, G.Q. Li, (e, 2e) electron momentum spectrometer with high sensitivity and high resolution, Rev. Sci. Instrum. 76 (6) (2005) 063103, https://doi.org/10.1063/1.1897668.
[23] X.-G. Ren, C.-G. Ning, J.-K. Deng, S.-F. Zhang, G.-L. Su, B. Li, X.-J. Chen, A high-efficiency electron momentum spectrometer for direct imaging of orbital electron density, Chin. Phys. Lett. 22 (6) (2005) 1382 URL: http://stacks.iop.org/0256-307X/22/i=6/a=023.
[24] C.-G. Ning, S.-F. Zhang, J.-K. Deng, K. Liu, Y.-R. Huang, Z.-H. Luo, Improvements on the third generation of electron momentum spectrometer, Chin. Phys. B 17 (5) (2008) 1729 URL: http://stacks.iop.org/1674-1056/17/i=5/a=032.
[25] M.F. Frisch, G.W. Trucks, H.B. Schlegel et al., Gaussian03 Revision E.01, gaussian Inc. Wallingford CT, 2004.
[26] N. Watanabe, X. Chen, M. Takahashi, Interference effects on (e, 2e) electron momentum profiles of cf_4, Phys. Rev. Lett. 108 (2012) 173201, https://doi.org/10.

1103/PhysRevLett.108.173201.
[27] E. Wang, X. Shan, Q. Tian, J. Yang, M. Gong, Y. Tang, S. Niu, X. Chen, Imaging molecular geometry with electron momentum spectroscopy, Sci. Rep. 6 (2016) 39351, https://doi.org/10.1038/srep39351.
[28] H. Nakatsuji, Multireference cluster expansion theory: Mr-sac theory, J. Chem. Phys. 83 (2) (1985) 713–722, https://doi.org/10.1063/1.449485.
[29] H. Nakatsuji, Exponentially generated wave functions, J. Chem. Phys. 83 (11) (1985) 5743–5748, https://doi.org/10.1063/1.449650.
[30] H. Nakatsuji, Exponentially generated configuration interaction theory. descriptions of excited, ionized, and electron attached states, J. Chem. Phys. 94 (10) (1991) 6716–6727, https://doi.org/10.1063/1.460248.
[31] J. Harvey, R.P. Tuckett, A. Bodi, Shining new light on the multifaceted dissociative photoionisation dynamics of ccl4, Phys. Chem. Chem. Phys. 16 (2014) 20492–20499, https://doi.org/10.1039/C4CP03009E.
[32] K.L. Nixon, A.J. Murray, O. Al-Hagan, D.H. Madison, C. Ning, J. Phys. B: Atomic Mol. Opt. Phys. 43 (3) (2010) 035201, https://doi.org/10.1088/0953-4075/43/3/035201.
[33] M. Gong, X. Li, S.B. Zhang, S. Niu, X. Ren, E. Wang, A. Dorn, X. Chen, Multicenter three-distorted-wave approach to three-dimensional images for electron-impact-ionization dynamics of molecules: overall agreement with experiment, Phys. Rev. A 98 (2018) 042710, https://doi.org/10.1103/PhysRevA.98.042710.
[34] N. Watanabe, M. Takahashi, Y. Udagawa, K.A. Kouzakov, Y.V. Popov, Two-step mechanisms in ionization-excitation of he studied by binary (e,2e)) experiments and second-born-approximation calculations, Phys. Rev. A 75 (2007) 052701, https://doi.org/10.1103/PhysRevA.75.052701.
[35] X. Ren, S. Amami, O. Zatsarinny, T. Pflüger, M. Weyland, A. Dorn, D. Madison, K. Bartschat, Kinematically complete study of low-energy electron-impact ionization of argon: Internormalized cross sections in three-dimensional kinematics, Phys. Rev. A 93 (2016) 062704, https://doi.org/10.1103/PhysRevA.93.062704.
[36] X. Ren, T. Pflüger, J. Ullrich, O. Zatsarinny, K. Bartschat, D.H. Madison, A. Dorn, Low-energy electron-impact ionization of argon: three-dimensional cross section, Phys. Rev. A 85 (2012) 032702, https://doi.org/10.1103/PhysRevA.85.032702.
[37] X. Ren, S. Amami, K. Hossen, E. Ali, C. Ning, J. Colgan, D. Madison, A. Dorn, Electron-impact ionization of at low projectile energy: Internormalized triple-differential cross sections in three-dimensional kinematics, Phys. Rev. A 95 (2017) 022701, https://doi.org/10.1103/PhysRevA.95.022701.